Design of a mobile flywheel energy storage driven by a switched reluctance machine

Fabian LORENZ*, Ralf WERNER*

* Chemnitz University of Technology, Faculty of Electrical Engineering and Information Technology

Chair of Electrical Energy Conversion Systems and Drives

Reichenhainer Straße 70, 09126 Chemnitz, Germany

E-mail: fabian.lorenz@etit.tu-chemnitz.de

Abstract

The rising number of hybrid and fully electrical driven cars requires more powerful short term energy storages to recover the breaking energy, especially in urban traffic. This paper presents a mobile flywheel energy storage system (FESS) designed for the use in mobile applications like passenger cars. The system is equipped with a carbon fiber composite flywheel connected to two switched reluctance machines which both can operate as motor and generator. The storage capacity is $190\,Wh$ at an overall weight of $64\,kg$. The peak power of the system is $24\,kW$. The construction of the flywheel will be outlined considering a stress distribution up to $30\,000\,rpm$ as well as rotordynamic concerns including the bearing concept. The system carries hybrid super precision roller bearings in a paired (tandem) configuration equipped with adjustable preloading and direct water cooling. Switched reluctance machines (SRMs) show great advantages in flywheel applications such as wide speed range, high reliability, and a robust rotor structure. The modelling process for the driving SRMs will be presented including the simulation workflow as well as results for key operation points.

Keywords : Flywheel energy storage, electric vehicles, switched reluctance machine, high speed, hybrid roller bearings

1. Introduction

With the rising number of hybrid and fully electrical driven vehicles the demand of powerful energy storage systems is increasing significantly. Most existing car concepts use Li-ion batteries which have a high energy density and show good performance if used at moderate levels of charging/discharging current. Especially in urban traffic, which is commonly the field of operation for electric cars, the load profile is very demanding because of the fast sequence of acceleration and breaking events. The resulting current peaks can lead to a remarkable reduction of the life span of the batteries (Bolund, et al., 2007), which still represent a major part of overall vehicle costs. A possibility to overcome this problem is the use of an additional high power short term storage to efficiently recuperate the breaking energy. Advanced flywheels can be a competitive alternative to the currently applied capacitors thanks to the availability of high strength materials and hybrid super precision roller bearings. The main advantages of flywheel energy storage systems (FESS) are high power density, wide range of operation temperature, and the absence of capacity degradation (Bolund, et al., 2007). The design of flywheel energy storages is a very complex task that is influenced by dozens of parameters. Numerous tradeoffs are necessary to find suitable dimensions for the main subsystems like the flywheel, the bearings and the driving machines, regarding storable energy, power and costs (Hedlund, et al., 2015). Especially the bearing concept in mobile applications is crucial for the performance of the FESS due to the gyroscopic reaction torques resulting from the vehicle movement. This paper concerns the complete design of a mobile flywheel energy storage specified for passenger cars with special regard to flywheel design and the driving switched reluctance machines.

2. System configuration

The goal of the system design is the minimization of weight and volume at a given storage capacity and power. The system carries a carbon fiber wound flywheel equipped with two switched reluctance machines which can both operate as motor (charging) and generator (discharging), mounted on one central shaft supported by super precision hybrid ball bearings. The housing is built up from steel and aluminum components to provide active water cooling for the driving machines as well as for the bearings, and meets sufficient safety requirements in case of failure of the flywheel hub. To reduce the aerodynamic drag of the flywheel, the housing is completely sealed in order to reduce the inside air pressure.
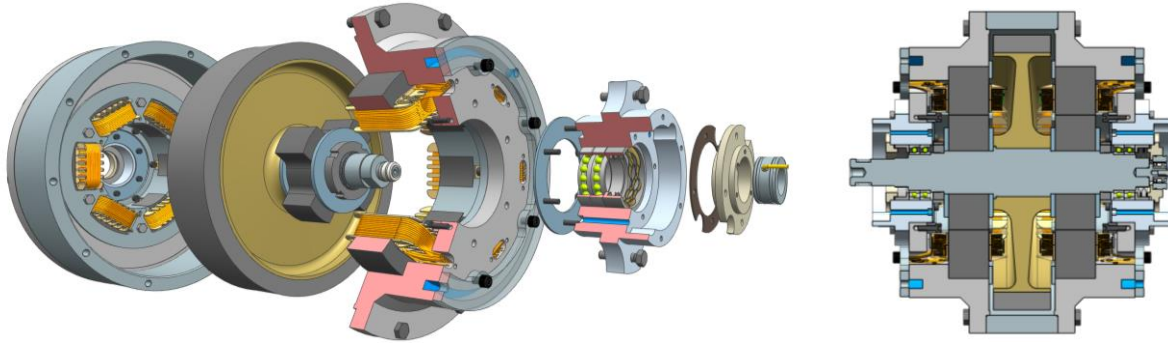

Fig. 1   Complete flywheel system in exploded (left) and cross-sectional (right) view

The presented design allows for a symmetric arrangement of the flywheel between the bearings and a very short shaft by optimally using the available installation space. Regarding the rotordynamic behavior this configuration comes close to the jeffcott rotor and allows a decoupled treatment of the tilting and bending frequencies of the flywheel (Gasch, et al., 2006). A further advantage of such symmetrically disc shaped rotors is the impact of the gyroscopic effect, which shifts the tilting eigenfrequencies to higher rotation speeds (Gasch, et al., 2006). The system is equipped with sufficient stiffness to stay in a subcritical mode over the whole range of operation. This is strongly recommended to avoid an uncontrolled spinning of the rotor near critical speeds.

Table 1   Flywheel system characteristics

Storable Energy	$190\ Wh$
Max. rotational speed	$30000\ min^{-1}$
Max. power	$24\ kW$
Weight	$64\ kg$
Dimensions	$360\ mm\ x\ 335\ mm$
Volume	$0.034\ m^3$
Charging time at max. power	$65\ s$

Figure 2   Storable energy as a function of the rotation speed
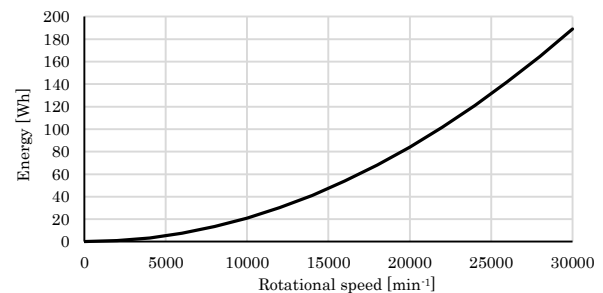
The bearing concept was designed in consideration of the reaction forces of the rotor which are induced by the vehicle movement. Apart from the translational accelerations, the angular movements can cause immense reaction torques in the flywheel rotor because of the gyroscopic effect, which was intensively analyzed in a previous publication (Lorenz and Werner, 2013). Neglecting the steering movements (yaw) by vertically arranging the rotor axis in the car, the bearing forces can still reach values up to $2000\ N$ caused by the pitch and roll movement. The use of active magnetic bearings with their indisputable advantages in high speed applications would result in a sharp increase of the system's weight, size and costs, as the bearings have to be very powerful to prevent an emergency touch down in all possible driving scenarios (Reicheis, et al., 2013). The applied hybrid angular contact ball bearings show far higher load ratings and have more robust characteristics in the harsh automotive environment. The bearings are installed in a paired DT (tandem) configuration. The bearing carrier provides adjustable preloading in order to influence the dynamic behavior of the rotor as well as active water cooling to prevent thermal overloading of the bearings.

Table 2 Bearing parameters (NSK, 2015)

Bearing type	NSK 40 BNR19X	Max. speed	$41\ 200\ min^{-1}$
Inner diameter	$40\ mm$	Stiffness	$190\ N/\mu m - 390\ N/\mu m$
Outer diameter	$62\ mm$	Lubrication	Grease

3. Flywheel design

To achieve the required storage capacity at minimum weight, disc shaped rotors made of materials with a high specific energy (ratio of yield strength to mass density) show good performance (Genta, 1985). The storable energy is linearly dependent on the polar moment of inertia Θ_p and quadratically on the rotational speed ω (Eq. 1), thus the rotational speed should be as high as possible (Genta, 1985).

$$E_{kin} = \frac{1}{2} J \omega^2 \tag{1}$$

Demanding requirements such as high temperature operation, benign burst behavior, predictability of stress distribution, and workable manufacturing have to be taken into account. Metals like tempering steel, aluminum 7075 or titanium alloys have moderate specific energies, are well suited for high temperature operation and their material properties are well predictable. The devastating burst behavior of full metal flywheels, however, enforces heavy containment structures and high security factors (Genta, 1985). High strength fiber composites have significantly higher specific energies and their material properties can be varied by arranging the fiber orientation (Arwin and Bakis, 2006). Especially the benign burst behavior makes them interesting for mobile flywheel applications but their poor heat resistance as well as the complex strength calculation have to be considered. The presented flywheel is made of a high strength steel hub that is press-fitted on the central shaft. The hub carries a circumferentially wound carbon fiber ring which is wound under prestress directly on the hub (Fig. 3).
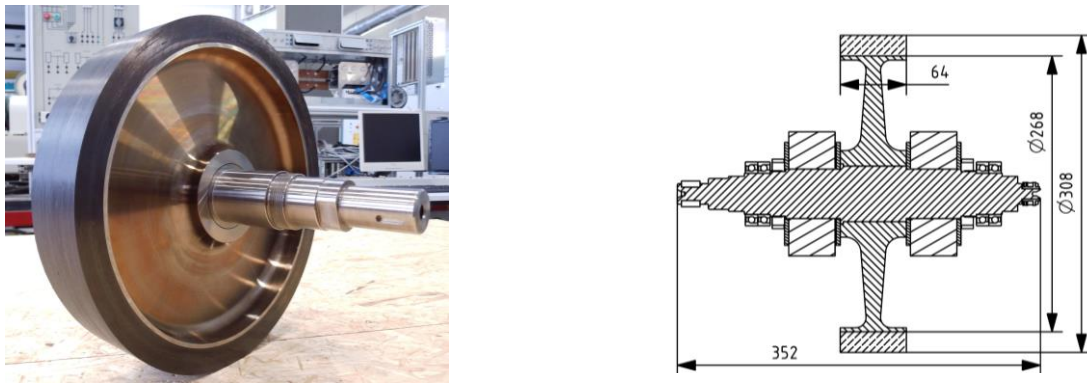

Figure 3 Assembled flywheel (left) and cross-sectional view of the rotor structure (right)

The shaft as well as the hub are made of standard steel grades which are widely available and easily machinable. The parts were very accurately processed down to tolerance class IT 4 to reduce the rotor imbalance to a minimum and to ensure a correct mounting of the bearings, which is crucial for their lifetime. Table 3 shows the used materials and their most important properties (Mitsubishi, 2015), (Ebalta, 2015), (Böhler, 2015), (Dörrenberg, 2015).

Table 3 Material properties of the flywheel components

Material	Tensile strength [MPa]	Tensile modulus [GPa]	Mass density [g/cm³]
Steel 1.7225 42CrMo8 (shaft)	650	210	7.72
Steel 1.6580 30CrNiMo8 (hub)	900	210	7.76
Carbon Fiber Dialead K63712	2600	640	2.12
Epoxy Resin Ebalta LH30	68	3.1	1.08
Composite (65% fibre volume content)	1710	410	1.76

Prestressing the flywheel can significantly increase the energy density by inducing residual radial compressive stresses which counteract the centrifugal loads at high speeds (Arwin and Bakis, 2006). Therefore, the press-fit of the hub on the shaft was designed very tightly with an offset of $0.12\ mm$, which charges the inner bore of the hub already up to 50% of its yield strength at stand still. Further residual stresses were brought in by winding a high modulus carbon fiber rim under a tension of $200\ N$ directly on the hub. The calculation of the stress distribution in such structures can be very demanding because of the stress conditions between the individual components, the orthotropic material properties of unidirectional wound fiber composites, and the complex shape of the hub. The stress analysis cannot be carried out in a completely analytical way, therefore, numerical methods have to be deployed. An appropriate way of modeling is the dissection of the carbon fiber rim in thin rings with a constant prestress resulting from the winding tension (Burg, 1996).

With d_B representing the thickness of the ring the radial pressure can be calculated from Eq.(2).

$$\sigma_\perp(r_W) = \sigma_\parallel(r_W) \cdot \frac{d_B}{r_W} \qquad (2)$$
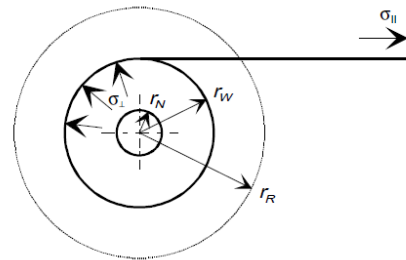
$$r_N \leq r_W \leq r_R \qquad (3)$$

Figure 4 Prestressing of the rotor by winding under tow tension (Burg, 1996)

Modelling a circumferential preload in a ring might be rather challenging but the resulting radial stress $\sigma_\perp$ can also be replaced by a suitable press-fit, which is a common feature in most finite element software. Numerous designs have been investigated to find a feasible solution that not only meets the required energy density but also considers the limitations of manufacturing. Especially the shaft-hub press-fit has to be designed primarily with respect to the joining process which is a very risky step of production. Figure 5 shows the calculated stress distribution and the contact pressures at the inner and outer diameter of the hub at a speed of $25000\ min^{-1}$ exemplarily. The highest stresses appear at the central bore of the hub and decrease with growing radius. The rim carries much higher loads than the outer diameter of the hub and acts as a support for the flywheel. Due to the high tensile modulus and very low mass density of the carbon fiber composite, the rim has a far smaller strain under centrifugal load than the steel hub whereby it reduces the elongation of the hub and thus reduces the occurring stresses in the center.
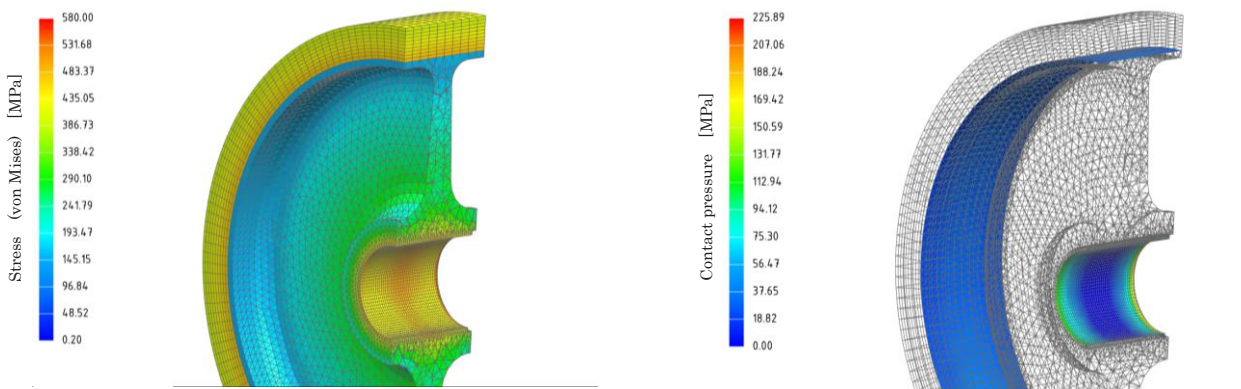

Fig. 5 Stress distribution in the flywheel hub and rim at $25000\ min^{-1}$ (left), contact pressure at the inner and outer diameter of the hub at $25000\ min^{-1}$ (right)

The chart in Fig. 6 shows the averaged stress values at the bore of the hub and the inner diameter of the rim as well as the contact pressures at these surfaces over the speed of the flywheel.
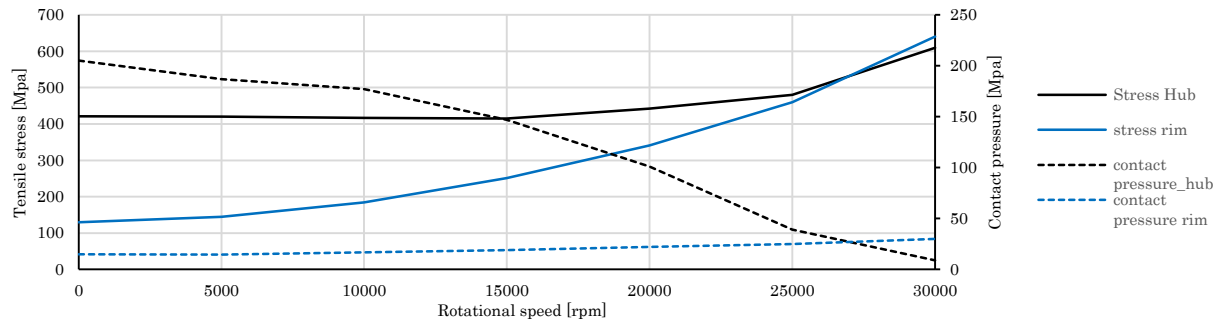
Figure 6   Averaged stress and contact pressure over speed for the bore of the hub (black) and the inner diameter of the rim (blue)

Evidently, the stress in the rim is rising much steeper with increasing speed compared to the stress in the hub which shows the shifting of the centrifugal loads from the hub to the rim. Despite of that the contact pressure of the hub-shaft connection is decreasing rapidly which is the limiting parameter for the flywheel speed. However, the averaged contact pressure comes close to zero the flywheel does still not lose contact to the shaft due to the wide shaped center of the hub whose outer edges maintain sufficient pressure values even at high speeds. A detailed view is provided in Fig. 5. A higher preloading of the rim is definitely preferable to improve the performance of the flywheel, however, this could not be realized with the available winding machine.

4. Design of switched reluctance machines

The application in mobile flywheel energy storages presents quite challenging boundary conditions regarding the choice of the driving machines. To achieve a competitive performance of the overall flywheel system, specific properties like very high speed capability, robust rotor construction, high reliability, and very low standby losses at high rotation speeds are required. Switched reluctance machines (SRMs) have superior characteristics meeting these requirements compared to permanent magnet synchronous machines and induction machines. Additionally, SRMs provide excellent field weakening capabilities at high speeds and are well suited for mass production due to their simple structure. Especially the low rotor losses regarding the poor cooling possibilities under reduced air pressure are particularly important. A switched reluctance machine (SRM) in 6/4 configuration was chosen as motor/generator for the flywheel system. Two identical machines are installed on both sides of the flywheel to achieve a symmetrical rotor structure. As a consequence of the salient pole structure and the pulsed winding excitation, the chosen 6/4 configuration produces a significant torque ripple, which is acceptable due to the high inertia of the flywheel but can produce high noise levels induced by vibrations of the lamination stack. To reduce the deformation of the stator by magnetic forces, the back iron is press-fitted into the housing which carries a special structure that tightly clamps the top ends of the stator teeth. Furthermore, the housing provides active water cooling to the stator where the major losses of the machine occur. Figure 7 gives a detailed view on the SRM, the housing, and the cooling concept, while table 4 lists the main parameters of the machine.

Table 4   Machine characteristics

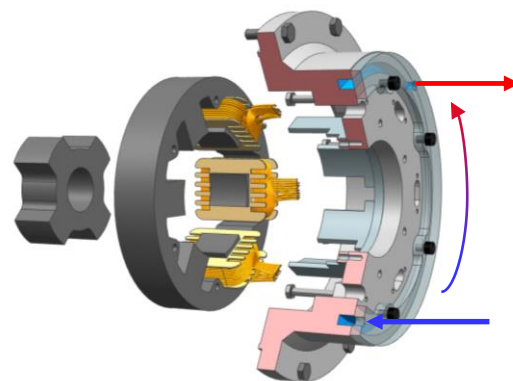|	
Stator phases	3
Phase voltage	$600\ V$
Speed range	$0\ -\ 30000\ min^{-1}$
Power	$12\ kW$ at $14000\ min^{-1}$
Winding peak current	$400\ A$
Lamination steel	M270-35A
Stator outer diameter	$237\ mm$
Rotor outer diameter	$128\ mm$
Stack length	$45\ mm$
Air gap length	$0.2\ mm$
Insulation class	F (155 °C)

Figure 7   Exploded cross-sectional view of the driving SRM (arrows showing the coolant flow)

SRMs are considerably simple electric machines but their behavior is difficult to model due to strong nonlinearities like saturation effects of the magnetic circuit and the variable inductance because of the doubly salient pole structure. The determination of the machine behavior requires the simulation of the electromagnetic system over the whole range of operation. The design of the driving SRMs for the presented flywheel system was carried out by using a combination of stationary finite element analysis (FEA) of the magnetic circuit and a transient numerical simulation of the electric circuit. The initial step is the calculation of the flux linkage $\Psi = f(i, \gamma)$ and static torque $T = f(i, \gamma)$ for one excited stator phase which are both dependent on the phase current i and rotor position γ. The characteristic function of the flux linkage can be regarded as the individual footprint of the SRM (Miller, 2001) and is the basis for further derivation of inductance and the back EMF. Figure 8 and 9 show the calculated characteristic graphs for the flux linkage and torque over an angular range of $0 - 45°$ which represents one stroke of the machine.
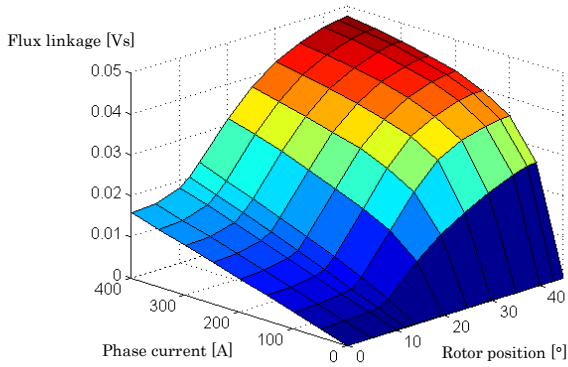

Figure 8   Flux linkage vs. rotor position and phase current
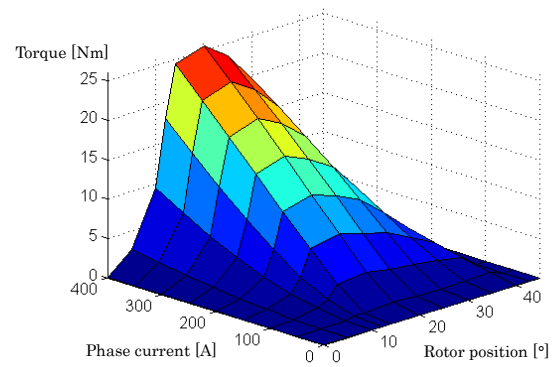

Figure 9   Torque vs. rotor position and phase current

To calculate the instantaneous torque of the rotating SRM, the voltage equation can be used to determine the instantaneous phase current.

$$v(i, \gamma) = R \cdot i + \frac{\partial \Psi(i, \gamma)}{\partial i} \cdot \frac{di}{dt} + \frac{\partial \Psi(i, \gamma)}{\partial \gamma} \cdot \frac{d\gamma}{dt} \tag{3}$$

The phase voltage consists of the resistive voltage v_r (first term), the inductive component v_i (second term) and the back EMF v_b (third term) (Miller, 2001) and was implemented in a transient Matlab/Simulink model in which the partial derivations of the flux linkage $\frac{\partial \Psi(i, \gamma)}{\partial i}$ and $\frac{\partial \Psi(i, \gamma)}{\partial \gamma}$ are represented by look-up tables. The model calculates the current in the phase windings which can be used with an additional look-up table to determine the instantaneous torque.
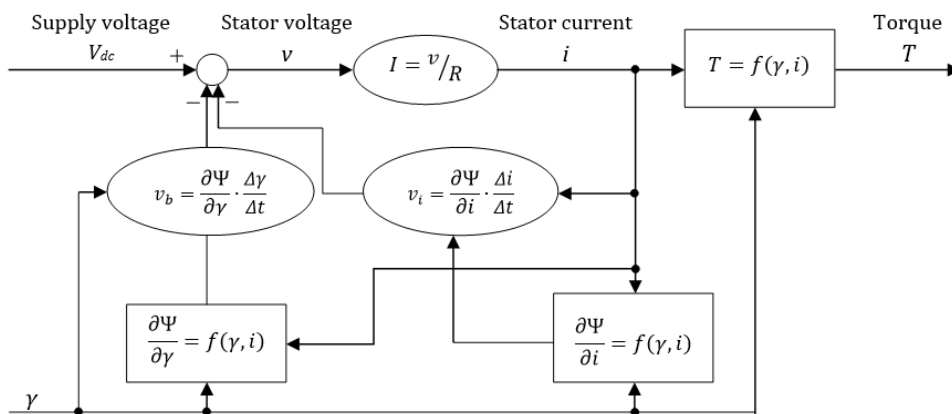

Figure 10   Structure of the transient model calculating the instantaneous current and torque of one single phase considering the switching angle and rotor movement

The performance of the machine is significantly affected by the switching angles of the phase voltage. Their values can be defined following issues according the efficiency of the machine, maximum torque, or the size of the torque ripple. Figure 11 shows the power output of the driving SRM using control parameters which aim on a maximum torque output and thus represent the maximum power of the machine. Defining the switching angles with respect to higher efficiencies and better power quality results in a derating of the output power. The consideration of the charging behavior of the flywheel system vs. time has been carried out using the maximum power control parameters. Figure 12 shows a complete charging cycle taking the operation of both SRMs into account.
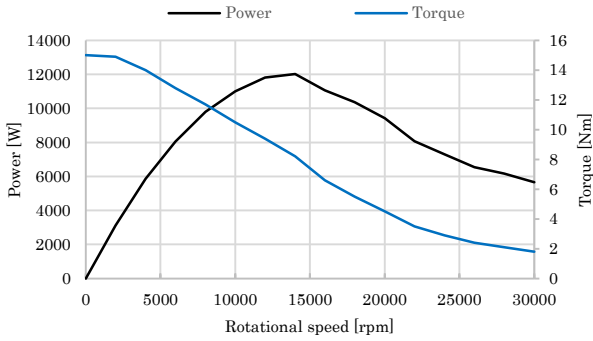
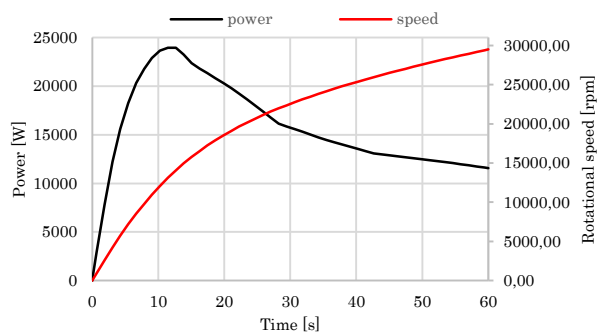

Figure 11   Power and Torque of one driving SRM vs. speed

Figure 12 Charging cycle of the flywheel system (2 SRMs), power and speed are plotted vs. time

5. Conclusion

The proposed flywheel energy storage system is designed for the use in mobile applications to store a kinetic energy of $190\ Wh$ providing a maximum power of $24\ kW$. The analysis of the stress distribution of the carbon fiber composite flywheel was carried out proving a speed capability of $30000\ min^{-1}$. The driving switched reluctance machines show great advantages for the application in mobile flywheel systems due to their wide speed range, robust rotor construction, and low standby losses. The overall system was designed to achieve a high reliability in combination with low production costs.

The system was assembled and is currently installed on a test bench (Fig. 13 and Fig. 14). In the next step, the power inverter has to be designed providing sufficient volt-amperes to prove the system performance over the whole range of operation.
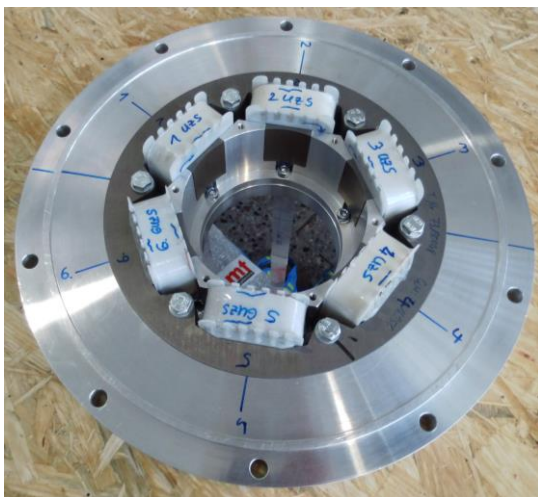

Figure 13   Assembled SRM in the housing

Figure 14   Flywheels system on the test bench

References

Arwin, A., Bakis,C., Optimal design of press-fitted filament wound composite flywheel rotors, Composie structures 72 (2006), pp. 47-57

Bolund, B., Bernhoff, H., Leijon, M., Flywheel energy and power storage systems, Renewable and Sustainable Energy Reviews, 11 (2007), pp.235-258.

Böhler, V45, Steel 1.6580 30CrNiMo8, (online), available from *http://www.dew-stahl.com/fileadmin/files/dew-stahl.com/documents/Publikationen/Werkstoffdatenblaetter/Baustahl/1.6580_de.pdf,* (accessed on 27 May, 2016)

Burg, P., Fast-rotating Flywheel made of fiber reinforced plastics, Diss. Techn. Wiss. ETH Zürich, Nr. 11444, 1996. (in german)

Dörrenberg, M4S, Steel 1.7225 42CrMo4, (online), available from *<http://www.doerrenberg.de/uploads/tx_c1x1downloads/1.7225_en.pdf>,* (accessed on 27 May, 2016)

Ebalta, LH30 Resin+hardener, (online), available from *<http://www.ebaltadistribution.co.uk/support/downloads/product_datasheets/lh/datasheet_uk_lh30a_b.pdf>,* (accessed on 27 May, 2016)

Gasch, R., Nordmann, R., Pfützner, H., Rotordynamics, Springer-Verlag, 2006. (in german)

Genta,G., Kinetic energy storage, Butterworth & Co, 1985

Hedlund, M., Lundin, J., Santiago, J., Abrahamsson, J. and Bernhoff, H., Flywheel Energy Storage for Automotive Applications, Energies 2015, 8(10), pp.10636-10663.

Lorenz, F. and Werner, R., Comparison of magnetic bearings and hybrid roller bearings in a mobile flywheel energy storage, Proceedings of the 1st Brazilian Workshop an Magnetic Bearings, 2013

Miller, T J E., Electronic control of switched reluctance machines, Newnes Power Engineering Series, 2001

Mitsubishi Chemical, Carbon fiber Dialead PD6371, (online), available from *<http://www.mitsubishichemical.com/DataSheets/CarbonFiber/PD%20K63712.pdf>*, (accessed on 15 May, 2016).

NSK Ltd., Super Precision Bearings, (online), available from *<www.jp.nsk.com/app01/en/ctrg/index.cgi?rm=pdfDown&pno=E1254>,* (accessed on 27 May, 2016).

Reicheis, M., Buchroithner, A., Andrasec, I., Gallien, T., Schweighofer, B., Bader, M. and Wegleiter, H., Improving kinetic energy storage for vehicles through the combination of rolling element and active magnetic bearings, IECON 2013 – 39th Annual Conference of the IEEE, pp.4641-4646.